Latitude-dependent nature and physical characteristics of transverse aeolian ridges on Mars

Sharon A. Wilson[1] and James R. Zimbelman

Center for Earth and Planetary Studies, National Air and Space Museum, Smithsonian Institution, Washington, DC, USA

Received 5 February 2004; revised 25 June 2004; accepted 6 August 2004; published 7 October 2004.

[1] Narrow-angle images from the Mars Orbiter Camera (MOC) have revealed the common occurrence of small-scale (<100 m wavelength) bright transverse aeolian ridges (TARs) on the surface of Mars. MOC images were used to assess the broad distribution of TARs from 90°N to 90°S between 180°E and ~240°E to investigate their relationship to latitude, elevation, thermal inertia, geologic units, local slopes, and surface roughness. Out of 5112 examined images from the primary mission, 520 (10%) contain evidence of TARs, 92% of the images with TARs are located between ±50° latitude, and very few occur in the middle to upper latitudes or polar regions of either hemisphere. TARs are observed at elevations from −5 km to 3 km, with the highest frequency (26%) between −1 and 0 km. There is no systematic relationship between the distribution of TARs and global thermal inertia measurements. Most TARs occur in geologic units associated with the Channel System Materials (39%) and the Olympus Mons Aureole (33%). At a length scale of 1.85 km/pixel, the average local slopes for images with and without TARs are 1.92° and 1.36°, respectively. Of the parameters investigated, the latitudinal trend of TARs in both hemispheres appears to be predominantly related to surface roughness, with a positive linear correlation between the surface roughness of geologic units and frequency of TARs ($R^2 = 0.87$). Factors affecting the semiglobal distribution of TARs are likely related to the climate and wind regimes in which they formed but do not provide definitive evidence for either saltation or reptation formation mechanisms. *INDEX TERMS:* 6225 Planetology: Solar System Objects: Mars; 5415 Planetology: Solid Surface Planets: Erosion and weathering; 5460 Planetology: Solid Surface Planets: Physical properties of materials; 5464 Planetology: Solid Surface Planets: Remote sensing; *KEYWORDS:* dunes, granule, ripple

Citation: Wilson, S. A., and J. R. Zimbelman (2004), Latitude-dependent nature and physical characteristics of transverse aeolian ridges on Mars, *J. Geophys. Res.*, *109*, E10003, doi:10.1029/2004JE002247.

1. Introduction

[2] Aeolian processes are significant in the geomorphology of planets with atmospheres and are likely the dominant surface-modifying process on Mars today. Orbital missions over the past three decades have returned increasingly detailed images of the Martian surface, revealing progressively smaller types of aeolian bedforms. Images from Mariner 9 in 1971–1972 had sufficient spatial resolution (~60 m/pixel) to allow the identification of large, low-albedo dune masses [*McCauley et al.*, 1972; *Sagan et al.*, 1972; *Cutts and Smith*, 1973; *Breed*, 1977]. Later high-resolution Viking Orbiter images (8–40 m/pixel) showed additional evidence for dark dune masses [e.g., *Cutts et al.*, 1976; *Breed et al.*, 1979] and also showed smaller, dune-like bedforms with the same relative albedo as their surroundings [*Ward et al.*, 1985; *Peterfreund*, 1985; *Zimbelman*, 1987; *Edgett*, 1997; *Zimbelman*, 2000]. Since 1997, the Mars Orbiter Camera (MOC) on Mars Global Surveyor (MGS) has returned thousands of narrow-angle (NA) images with a maximum resolution of 1.5 m/pixel [*Malin et al.*, 1992, 1998; *Malin and Edgett*, 2001]. The vastly improved resolution and surface coverage of MOC NA images has revealed the common occurrence of small-scale (wavelength <100 m), transverse aeolian bedforms that are morphologically distinct from the massive, low-albedo dunes observed decades prior [*Malin et al.*, 1998] (Figure 1). Hereafter referred to as "transverse aeolian ridges" (TARs) [*Bourke et al.*, 2003], these bedforms are interpreted to be either dunes or large ripples.

[3] Recent studies of TARs on Mars describe the characteristic morphology, albedo, thermal inertia and relationship to surrounding topographic features in isolated localities or regions [*Edgett*, 1997; *Malin et al.*, 1998; *Edgett and Parker*, 1998; *Thomas et al.*, 1999; *Edgett and Malin*, 2000b; *Malin and Edgett*, 2001; *Zimbelman and Wilson*, 2002; *Wilson and Zimbelman*, 2002; *Wilson et al.*, 2003; *Fenton et al.*, 2003]. The composition, age and formation mechanism of these aeolian bedforms are unknown, as are the global conditions in which they formed. The goal of this

[1]Now at the Department of Environmental Sciences, University of Virginia, Charlottesville, Virginia, USA.

Copyright 2004 by the American Geophysical Union.
0148-0227/04/2004JE002247$09.00

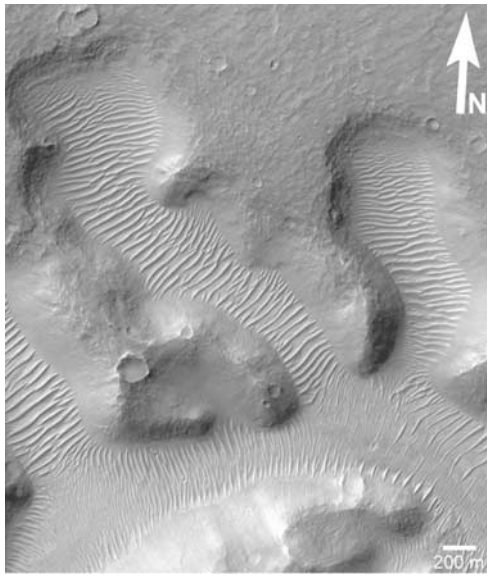

Figure 1. MOC NA image showing typical, light-toned TARs in Nirgal Vallis, near 27.83°S, 316.66°E, in E02-02651; illuminated from upper left. NASA/JPL/Malin Space Science Systems.

research is to systematically quantify the occurrence of TARs on a large spatial scale to examine their distribution in relation to latitude, elevation, thermal inertia, geologic units, local slopes and surface roughness. The investigation of global factors that affect the large-scale occurrence and latitudinal distribution of wind-related deposits may provide insight into the climate record [e.g., *Greeley et al.*, 2002], as well as the past and present-day wind regime on Mars.

2. Background

2.1. Terrestrial Aeolian Bedforms

2.1.1. Ripples, Dunes, and Draa

[4] Terrestrial aeolian deposits are commonly categorized as ripples, dunes or draa on the basis of bedform scale and grain size [*Wilson*, 1972a, 1972b]. The characteristic morphology and associated particle size indicate that each class has distinct formation, propagation and modification processes (summarized by *Greeley and Iversen* [1985], *Pye* [1987], *Pye and Tsoar* [1990], *Cooke et al.* [1993], and *Lancaster* [1995]).

[5] Ripples are the smallest aeolian bedforms and are ubiquitous on all sand surfaces except those undergoing rapid deposition [*Lancaster*, 1994]. Ripples exhibit wavelengths of 50–200 mm and amplitudes of 0.005–0.010 m [*Bagnold*, 1941; *Sharp*, 1963]. The lee slopes of ripples are less than the angle of repose (20–30°), and these bedforms have a ripple index (ratio of wavelength to height) of >10–15 [*Sharp*, 1963]. *Bagnold* [1941] interpreted ripple wavelength as a factor of saltation (short hops with relatively flat trajectories, from the Latin for "jump") path length but subsequent field observations [*Sharp*, 1963], laboratory experiments [*Seppälä and Linde*, 1978; *Walker*, 1981], computer simulations [*Werner*, 1988] and modeling [*Anderson*, 1987] suggest that ripple wavelength is more a function of reptation (surface creep, or the sediment load moved by traction, from the Latin for "crawl") path length and the microtopography of the surface.

[6] Documentation of desert dune forms dates to the late 19th century, but *Bagnold* [1941] was the first to quantify sand transport processes in relation to surface winds [*Lancaster*, 1995]. Dunes are fine-grained bedforms that form via saltation, and are typically characterized by a gentle stoss slope and a slip face on the lee side that reflects the angle of repose. Unlike ripples, dunes are generally more than tens of saltation path lengths long and are large enough to alter wind flow over them [*Bagnold*, 1941].

[7] The largest aeolian bedforms are draa, which are sheets of very large compound or complex dunes that generally exhibit spacing greater than 500 m [*Lancaster*, 1995]. Although draa are structurally analogous to dunes, on a large scale they are considered older and less mobile [*Cooke and Warren*, 1973].

2.1.2. Granule and Pebble Ripples

[8] Granule and pebble ripples on Earth are a rare transitional bedform that occur along the continuum between ripples and dunes [*Ellwood et al.*, 1975], and have been previously described as ripple ridges [*Bagnold*, 1941], granule ripples [*Sharp*, 1963; *Fryberger et al.*, 1992] and megaripples [*Greeley and Iversen*, 1985]. Although terrestrial dunes and ripples have distinct formation mechanisms, a plot of bedform wavelength versus particle size indicates the potential for overlap between bedform classes [*Wilson*, 1972b]. For example, large ripples and small transverse dunes can both occur with 1-meter wavelengths, but they are clearly differentiated by the size of the materials typically involved (e.g., meter-scale ripples contain much coarser particles than meter-scale dunes). Terrestrial granule and pebble ripples are defined by the size of their coarsest surface particles (coarse granules to very fine pebbles) and typically exhibit wavelengths that range from ~1 up to 20 m with amplitudes of tens of centimeters [*Greeley et al.*, 2002]. The largest ripples (wavelengths >5 m) have a surface coating of pebbles with diameters ranging from 0.4 to >1 cm [*Williams and Zimbelman*, 2002; *Williams et al.*, 2002]. Unlike typical impact or aerodynamic ripples, which form as a result of individual grains interacting with the wind, the formation of granule and pebble ripples is dominated by creep and traction, and they propagate as grains are nudged and/or rolled along by the impact of smaller, saltating grains [*Bagnold*, 1941; *Greeley and Iversen*, 1985]. As a result, these large ripples commonly occur in areas where the finer particles are deflated by the wind leaving behind a lag of coarser, denser grains [*Edgett*, 2002] concentrated along the ripple crest [*Sharp*, 1963; *Tsoar*, 1990] or in the trough [*Greeley and Iversen*, 1985; *Greeley et al.*, 2002]. On the basis of the physical characteristics and morphology of TARs on Mars as seen in MOC NA images, granule and pebble ripples have been identified as a viable terrestrial analog [*Malin and Edgett*, 2001; *Williams et al.*, 2002; *Zimbelman and Wilson*, 2002; *Wilson and Zimbelman*, 2002; *Wilson et al.*, 2003].

2.2. Transverse Aeolian Ridges on Mars

[9] The thin atmosphere on Mars leads to increased saltation path lengths of sand-sized particles [*White*, 1979], introducing the possibility of overlap between

the physical dimensions of large ripples and small dunes [*Bagnold*, 1941; *Anderson*, 1987; *Anderson and Haff*, 1988]. At the resolution of MOC NA images ($\geq$1.5 m/pixel), TARs on Mars cannot be definitively classified as ripples or dunes. As a result of the inherent ambiguity of these bedforms, they have been described as ripples or "ripple-like" bedforms [*Malin and Edgett*, 2001; *Zimbelman and Wilson*, 2002; *Williams et al.*, 2002; *Williams and Zimbelman*, 2002; *Wilson and Zimbelman*, 2002; *Wilson et al.*, 2003], "duneforms" [e.g., *Greeley et al.*, 2000; *Fenton et al.*, 2003] and dunes [*Malin et al.*, 1998; *Thomas et al.*, 1999].

2.2.1. Classification

[10] On the basis of descriptions of ripple-like features on Mars by *Malin and Edgett* [2001], *Zimbelman and Wilson* [2002] classified these small-scale aeolian bedforms into six categories using MOC NA images from Syrtis Major. This scheme is also applicable on a global scale (Figure 2).

[11] TARs commonly form "ripple bands" (Figure 2a) in depressions such as troughs, valleys and grabens [*Carr and Malin*, 2000; *Malin and Edgett*, 2001], where the crests are oriented perpendicular to the walls of the structure, presumably forming transverse to the local wind direction [*Malin and Edgett*, 2001]. They also occur on flat-lying surfaces (e.g., graben and crater floors, plains) as expansive "ripple fields" (Figure 2b), "large ripple patches" (Figure 2c), and small "isolated ripple patches" (Figure 2d). TARs that are refracted around the bases of topographic rises such as bedrock knobs, yardangs or dunes are described as "obstacle ripples" (Figure 2e). When dunes and TARs appear together, the TARs can be beneath, superposed on, or refracted around the base of the dune (Figure 2f). In most cases where dunes and ridges occur together, the darker dune material is seen overlying the TARs [*Malin and Edgett*, 2001]. In many images depicting this relationship, the bright aeolian ridges appear unaltered by the migration of dark dunes over them. This relationship suggests that TARs might be indurated or lithified to some extent, or the dunes and ridges vary in particle size and/or density [*Ward et al.*, 1985; *Edgett and Malin*, 2000b]. If the TARs are indeed analogous to granule or pebble ripples, they would be composed of larger and/or denser grains and would move more slowly than fine-grained dunes [*Edgett and Malin*, 2000b]. Less commonly, TARs are superposed on dunes or appear refracted around the base of a larger dune. Ridges that are superposed on dunes typically exhibit the same albedo as the underlying dune. Where TARs appear refracted around the base of a dune, the ridges were either formed after the dunes (and are therefore younger), or the ridges existed in that location before the dunes were formed (perhaps in a different orientation) and were remobilized due to increased divergence of wind flow around the dunes.

2.2.2. Albedo

[12] Albedo variations seen in MOC NA images, and the relationship between typical dark dunes and brighter TARs, suggest that there is a range of aeolian bedforms on the surface of Mars that vary in composition, physical make-up (i.e., particle size and density), as well as relative age and degree of mobility [*Malin et al.*, 1998; *Edgett and Parker*, 1998; *Edgett and Malin*, 2000b]. Because MOC images are not calibrated to yield a quantitative measure of albedo, the albedo of aeolian bedforms is described relatively as "darker" or "brighter" than the surroundings [*Edgett and Parker*, 1998; *Edgett*, 2002]. Typical dark dunes and dune fields on Mars have an albedo of <0.15 [*Cutts and Smith*, 1973; *Thomas and Weitz*, 1989] and are almost always composed of dark-toned material, unless they are covered by seasonal frost [*Malin and Edgett*, 2001]. Low-albedo dunes in Viking Orbiter images were thought to contain mafic material, such as basalt [*Bell et al.*, 1997], and remained dark because saltating sand particles prevented dust accumulation [*Thomas*, 1984; *Lee*, 1986].

[13] In MOC images, TARs exhibit a variety of albedo properties [*Edgett and Parker*, 1998], but they are generally brighter or have the same relative albedo as their surroundings. These bright bedforms have estimated albedo values of >0.21 up to about twice the albedo of dark dunes [*Edgett*, 1997; *Edgett and Parker*, 1998; *Thomas et al.*, 1999]. Brighter bedforms were originally interpreted as dust-covered [*Edgett*, 1997; *Zimbelman*, 2000], but further evidence from MOC images suggests that high albedo properties of these deposits cannot be attributed entirely to dust mantling and may instead be an indication of their composition [*Ward et al.*, 1985; *Malin et al.*, 1998; *Edgett and Malin*, 2000b], such as the bright sand hypothesis suggested by *Edgett and Parker* [1998].

2.2.3. Composition

[14] The composition of bright TARs remains uncertain. Because these bedforms are likely formed from local materials [*Fenton et al.*, 2003], the mineral assemblage may vary considerably depending on the environment in which the source material formed (e.g., lacustrine, volcanic). Average thermal inertia measurements of bright aeolian "duneforms" on the floor of Proctor Crater suggest an average size of medium to coarse sand, and may partially consist of basaltic material [*Fenton et al.*, 2003]. However, thermal inertia measurements at this location may be skewed by other factors, such as boulders and dust, or the bedforms may be a mixture of coarse material and finer sand that would yield the same thermal signature as medium sand. Thermal Inertia values of bright TARs from THEMIS (Thermal Emission Imaging System) data in Nirgal Vallis are indicative of moderate to coarse sand [*Zimbelman*, 2003]. A study of TARs (termed "bright dunes") by *Thomas et al.* [1999] proposed a composition of relatively soft materials, such as gypsum or other sulfates. In a study of TARs on the floor of a channel near Schiaparelli Basin, *Edgett and Parker* [1998] suggest that the ridges may contain minerals such as quartz or feldspar that would have been relatively resistant to chemical and mechanical weathering during the Noachian when fluid water may have occupied such a channel. Alternatively, the mineral assemblage at this location may be associated with evaporates and/or carbonates that would have precipitated from the proposed lacustrine environment.

2.2.4. Physical Characteristics

[15] In general, smaller aeolian bedforms exhibit smaller wavelengths, and larger bedforms have larger wavelengths [*Malin and Edgett*, 2001], but local topography appears to be a dominant factor in the size and shape of many aeolian

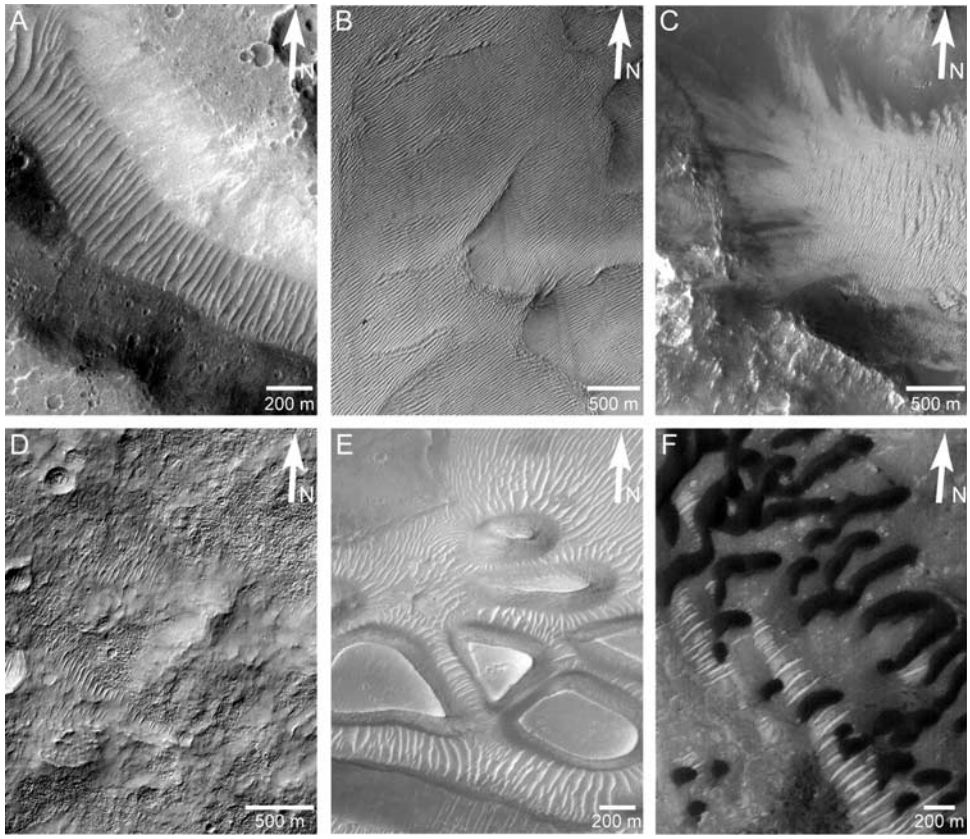

Figure 2. Classification scheme using examples of typical TARs as seen in MOC NA images. (a) ''Ripple band'' in Nirgal Vallis, near 27.59°S, 315.72°E, in E10-02335, illuminated from the left; (b) ''ripple field'' in Eastern Candor Chasma, near 7.44°S, 291.47°E, in E03-02283, illuminated from the left; (c) ''ripple patch'' along the Syrtis/Isidis transition zone, near 17.78°N, 75.75°E, in M04-02904, illuminated from left; (d) ''isolated ripple patches'' in the highland cratered terrain near 39.25°S, 219.38°E, in M00-02082, illuminated from the upper left; (e) ''obstacle ripples'' in East Candor Chasma near 6.0°S, 289.90°E, in E04-01514, illuminated from the left; (f) ''dunes and ripples'' in a crater near 10.96°N, 8.80°E, in SP1-26004, illuminated from the right. NASA/JPL/Malin Space Science Systems.

bedforms. *Wilson and Zimbelman* [2002] systematically examined 3400 images from Syrtis Major, Noachis, Memnonia and Phaethontis, and measured the physical characteristics of 340 transverse aeolian bedforms from 172 MOC NA images. The average wavelength of these bedforms is 40 m, typically ranging between ~10–60 m. The average length of the individual crests where wavelength measurements were obtained is 215 m (SD = 155 m). Little to no correlation was found between wavelength and crest length dimensions for any class of TARs (i.e., ripple band, ripple field, etc). Further examination of TARs in troughs less than 600 m wide, however, did yield a relationship between crest length and wavelength (R^2 = 0.63) [*Bourke et al.*, 2003]. Approximately 7% of TARs in the images examined from Syrtis Major have wavelengths of <15 m; the smallest resolvable TARs visible in MOC NA images have wavelengths of ~12–13 m. This observation, however, does not preclude the existence of smaller-wavelength bedforms on Mars; rather, it reflects the limitations in pixel resolution of MOC NA images and associated difficulty with distinguishing individual ridge crests. The Mars Exploration Rovers have detected numerous aeolian ripples with wavelengths from 0.2 to 1 m, some of which are composed of a bimodal particle size distribution [*Greeley et al.*, 2004].

[16] Although the exact heights of TARs observed in MOC NA images are unknown, estimates from several studies range from ~2 to ~6 m. A low-incidence-angle MOC image placed an upper height limit of 1.5 m for the aeolian ridges in Acheron Fossae [*Zimbelman*, 2000]. Using stereo pairs of MOC NA images, *Williams and Zimbelman* [2003] measured heights of ~5.7 m for TARs with wavelengths of roughly 38 m. *Bourke et al.* [2004a] estimated the minimum and maximum heights of TARs from three transects in Proctor Crater and a site near Gorgonum Chaos using profiling photoclinometry, measurements of slip face length (assuming 25°–30° for angle of repose) and stereography. Minimum and maximum heights from these methods across all sample locations range from 1 to 7.8 m (average minimum to maximum = 2.4 to 4.8 m). An analog study by *Wilson et al.* [2003] estimated the heights of the TARs on Mars by extrapolating the known physical dimensions of granule and pebble ripples and transverse dunes on Earth. The overall shape of the terrestrial deposits was normalized to a wavelength of 10 m, which roughly represents the smallest resolvable TARs seen in MOC NA images. On the basis of this linear extrapolation, if an average 40-meter wavelength aeolian bedform on Mars has heights of ~2.5 to 3.5 m, it would be

more analogous to granule or pebble ripples, whereas deposits analogous to transverse dunes would have heights closer to 1 m at a 40 m wavelength.

3. Procedure

[17] The Malin Space Science System (MSSS) and the Planetary Data System (PDS) websites were used to locate and systematically examine every MOC NA image released through the primary mission (acquired September 1997 through January 2001, AB1–M23) in Mare Boreum, Diacria, Amazonis, Memnonia, Phaethontis and Mare Australe (Mars Charts 1, 2, 8, 16, 24 and 30, respectively). The general area spans from 90°N to 90°S between 180°E to ~240°E. This process resulted in a total of 5112 MOC NA images examined (56% from southern hemisphere, 44% from northern hemisphere). The images were divided into two categories depending on whether they exhibited or lacked transverse aeolian ridges (TARs).

[18] ArcGIS (Geographic Information System) software was used to examine and analyze the distribution of all images, both with and without TARs, in relation to latitude, elevation, thermal inertia, geologic units and local slopes. The center latitude and longitude point of every image in the study area were plotted on a 64 pixel/degree Mars Orbiter Laser Altimeter (MOLA) grid (Figure 3). The latitudinal distribution of images in 10° bins, from 90°N to 90°S, were plotted separately.

[19] Elevation values for each image were also obtained from MOLA on the basis of the center latitude and longitude point of each image. The frequency of images with TARs was analyzed in 1 km elevation bins, and bins with less than 100 images were grouped with adjacent bins for the purpose of interpretation based on statistical significance.

[20] GIS and the digital global geologic map of Mars (based on maps produced by *Scott and Tanaka* [1986], *Greeley and Guest* [1987], and *Tanaka and Scott* [1987]) from the U.S. Geological Survey (USGS) Planetary GIS Web Server (PIGWAD) were used to determine the percentage of images with TARs in each geologic unit. The area of each geologic map unit in the study region was determined from a projected version of the geologic map. For simplicity, the geologic units were grouped into formations (Olympus Mons Formation, Channel System Materials, etc). Because the total number of images and the cumulative area of the geologic units in each geomorphic group vary, we report the area normalized image density, hereafter referred to as "image density." The image density is the total number of images in each formation divided by the cumulative area of all units within that formation. This parameter provides a relative sense of the proportion of the area covered by the images based on the assumptions that images are randomly obtained throughout all geologic units and the surface area of the examined MOC NA images is comparable to each other. Inferences about formations with relatively low image densities (i.e., few images per area) are associated with a higher level of uncertainty than those with higher image densities.

[21] GIS and a global thermal inertia map, representing physical characteristics of the surface including thermal conductivity, bulk density and heat capacity [*Mellon et al.*, 2000; *Putzig et al.*, 2003], was utilized to examine the relationship between the center point of images with TARs and thermal signatures within the study region.

[22] Local slope values at a baseline length of 1.85 km/pixel were determined for all images between ±60° on the basis of their center latitude and longitude points using a sinusoidal 32 pixel/degree digital elevation model (DEM). A two sample z-test for means was calculated to determine statistical significance.

4. Results

4.1. Latitudinal Distribution

[23] The systematic examination of 5112 images from 90°N to 90°S between 180°E to ~240°E revealed that 10% of the images exhibit TARs. Although this result confirms the prevalence of these aeolian bedforms on the surface of Mars, their latitudinal dependence (Figure 3) suggests these bedforms may not be as globally ubiquitous as previously suggested [*Malin and Edgett*, 2001].

[24] The frequency of TARs in 10° latitude bins reveals a latitude trend in both hemispheres (Figure 4). The average number of images in each 10° latitude bin is 284 (SD = 101), and the frequency of images with TARs ranges from 0–45% across all latitude bins. Almost all (92%) of the images with TARs are located between ±50°, with very few TARs in the middle to upper latitudes of either hemisphere, at the poles, or within the latitude bin from 0° to 10° north.

[25] Most (73%) of the images exhibiting TARs in the study region are located in the southern highlands, with the highest frequency (45%) between 30° and 40°S. Of the 379 images with TARs in the southern hemisphere, 69% occur between 10° and 40°S and 92% occur between 0° and 50°S. The frequency of images with TARs in the southern hemisphere decreases to ~1–3% in latitude bins poleward of 50°S. Of the 141 images with TARs in the northern hemisphere, 70% occur between 10° and 30°N and 90% occur between 0° and 40°N. Most (~60%) of the images with TARs in the northern hemisphere are associated with the Olympus Mons Aureole (10–40°N, ~210–230°E), with the remainder located west of Amazonis Planitia from 0° to 40°N in rough, fractured terrain such as the HNu (undifferentiated) unit in the Highly Fractured Materials, the Ridged Plains Materials (Hr) and the Arcadia Formation. We found very few examples of TARs in the northern lowlands; the frequency of images with TARs in the northern hemisphere decreases to 0–3% in latitude bins greater than 40°N.

[26] The dearth of images with TARs in the northern lowlands poleward of 40°N is a good indication that the particles comprising TARs are not derived from sediments associated with the hypothesized northern ocean [*Parker et al.*, 1989, 1993]. The small increase in the frequency of images with TARs (~3%) between 80° and 90°N in the linear dune material (Adl) and between 70° and 80°S in the polar layered deposits (Apl) suggests that an adequate sediment supply exists at these latitudes, along with sufficient wind velocities required to form TARs. The dramatic decrease in the prevalence of TARs in the polar regions relative to the equatorial region and the midlatitudes, however, may be the result of very low seasonal temperatures or frost cover that somehow restrict the

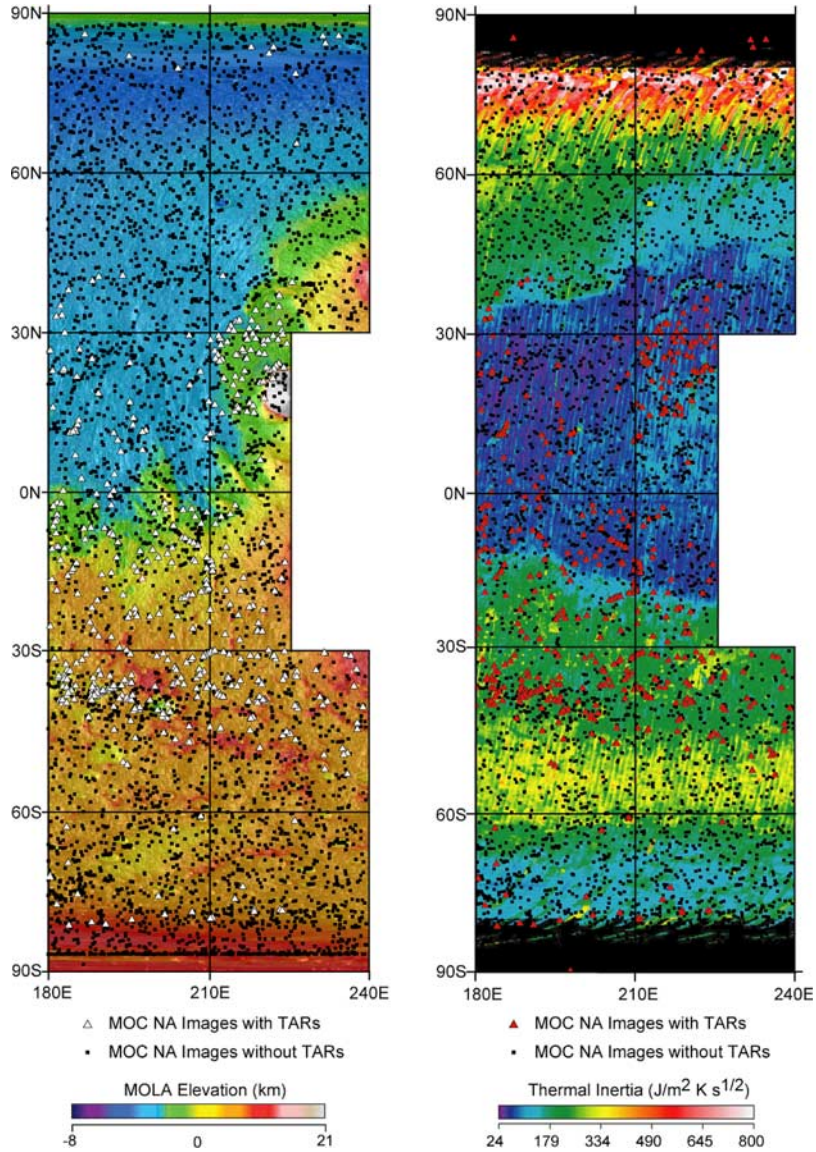

Figure 3. Latitudinal distribution of MOC NA images exhibiting (white or red triangles) and lacking (black squares) transverse aeolian ridges (TARs) in relation to MOLA elevation values (left) and global thermal inertia (right). The study region consists of six Mars Charts from 90°N to 90°S between 180°E and ~240°E and includes a data set of 5112 MOC NA images from the Primary Mission of Mars Global Surveyor.

mobility of the particles that comprise TARs, thus inhibiting their formation. The latitudinal dependence of images with TARs in this study region reflects changes in regional elevation and roughness (discussed in section 4.5), with the majority of ridges located at elevations above that of the northern lowlands.

4.2. Elevation

[27] The elevation values in our study region range from below −5 km to over 15 km relative to the MOLA datum [*Smith et al.*, 1999]. To compensate for the relative paucity of images in elevation bins below −5 km and above 3 km (average = 6 images per bin; SD = 15), the data were grouped into the following elevation bins: −6 to −4 km; +2 to 16 km; and 1 km bins from −4 km through +2 km (Figure 5). The average number of images in each elevation bin is 682 (SD = 341). Although the study region includes elevations from below −5 to over 15 km, the vast majority (98%) of the images examined occur between −5 km and +3 km. The frequency of images with TARs between −3 and +2 km is moderately enhanced (12−26%), with the highest concentration between −1 and 0 km (26%). The frequency of images with TARs significantly decreases to <6% at all elevations below −4 km and above +2 km. Of the 520 images with TARs, 97% are located at elevations between −4 and +3 km and 74% are found at elevations between −3 and +2 km.

[28] The thin atmospheric conditions on Mars should cause wind-blown material to be more mobile at lower elevations and under presumably higher atmospheric pressures. This study, however, shows that the processes responsible for forming TARs occurred over a wide range

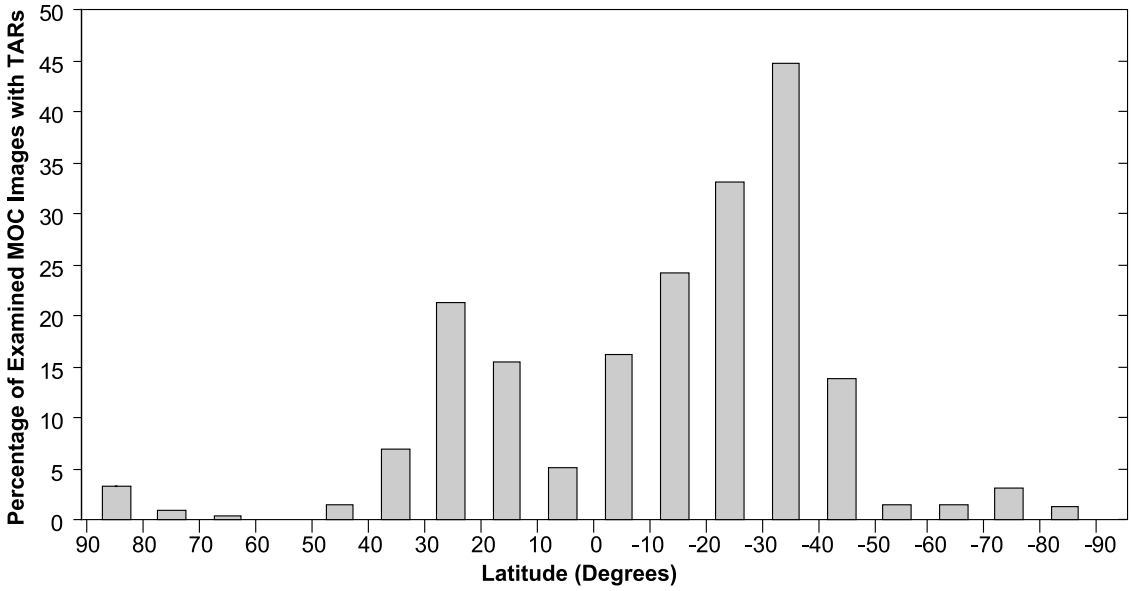

Figure 4. Percentage of examined MOC NA images with transverse aeolian ridges (TARs) from the Primary Mission of Mars Global Surveyor in 10° latitude bins from 90°N to 90°S latitude between 180°E and ~240°E.

of elevations on Mars, and most commonly at elevations above that of the northern lowlands. The abundance of TARs at low elevations above the northern lowlands (e.g., −3 km to +2 km) suggests that atmospheric pressure is not a limiting factor on TAR development over most or all of the study area. Of the 520 images with TARs, ~1% occur at elevations greater than 3 km, supporting the observation that aeolian processes do occur at high elevations and under presumably lower than current average atmospheric pressure [*Edgett and Malin*, 2000a; *Malin and Edgett*, 2001]. Elevations over 3 km may represent an effective upper limit to where the aeolian processes responsible for TARs can commonly occur. Alternatively, the atmospheric pressure at the time these high-elevation TARs formed may have been very different from present-day conditions due to changes in obliquity and global climate [e.g., *Head et al.*, 2003]. Additional examination of images at higher elevations is necessary to further explore the prevalence of TARs at elevations greater than 3 km to avoid sampling effects that may have occurred within the study region.

4.3. Thermal Inertia

[29] The map of global thermal inertia (TI) [*Mellon et al.*, 2000; *Putzig et al.*, 2003] provides insight into the physical characteristics of the Martian surface, as it relates to factors such as grain size, degree of induration, abundance of rock, and exposed bedrock. Generally, low TI values are associated with fine-grained and loosely packed material, whereas high TI values are related to rocks, indurated surfaces, and exposed bedrock.

[30] The majority of the study region contains TI values that range from low to moderate (~40–340 J m^{-2} $s^{-1/2}$ K^{-1}), with the highest values near the north pole (~500 J m^{-2} $s^{-1/2}$ K^{-1}). The lowest TI signature is between ~35°N to ~20°S, a region covered by broad dust deposits [*Mellon et al.*, 2002]. Higher TI signatures occur from ~35°N to 70°N and 20°S to 60°S, a region interpreted to consist of coarser soil, surface rocks, and some degree of indurated soils [*Mellon et al.*, 2002]. The images with TARs in the northern hemisphere (0°–40°N) correspond only to very low values of TI (~40 J m^{-2} $s^{-1/2}$ K^{-1}), whereas the TARs in the southern hemisphere are associated with TI values that range from ~40–255 J m^{-2} $s^{-1/2}$ K^{-1} (Figure 3). The increase in TI from ~180 to 330 J m^{-2} $s^{-1/2}$ K^{-1} between ~50° to 60°S correlates to the sudden decrease in the frequency of TARs in the southern hemisphere poleward of 50°S.

[31] Dust cover likely inhibits movement of particles by the wind, suggesting that TARs in low TI regions are older than the large-scale dust deposits. Although the dust layer may only be centimeters to decimeters thick, it is responsible for the observed low TI signatures but not sufficiently thick to mute the underlying topography, including the observed aeolian ridges. The age of the large-scale dust deposits is estimated to be 10^5–10^6 years on the basis of the estimated thickness and rate of accumulation [*Christensen*, 1986]. If the TARs in this region are older and therefore underlie the thin dust deposits that influence the regional TI signature, there is no temporal or material connection between the dust and the TARs. It is also possible that the lack of a clear relationship between the distribution of images with TARs and global TI signatures in the study region may be influenced by scale differences. The TI map was derived from surface temperature observations measured by the Thermal Emission Spectrometer (TES) at a resolution of ~3 × 6 km [*Mellon et al.*, 2002], which is much larger than the scale of the aeolian bedforms under consideration.

4.4. Regional Geology

[32] The study region contains a total of 53 geologic units as defined by *Scott and Tanaka* [1986], *Greeley and Guest* [1987], and *Tanaka and Scott* [1987]. The 520 images with TARs occur in 38 different geologic units. The 38 units

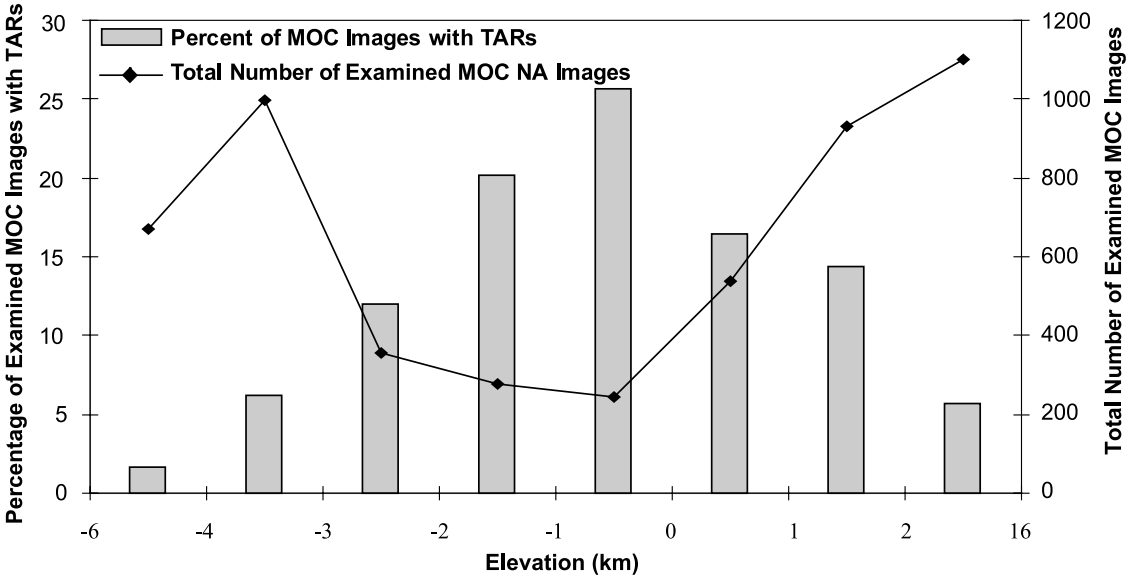

Figure 5. Percentage of examined MOC NA images with transverse aeolian ridges (TARs) (bars) and the total number of examined MOC NA images (line) from the Primary Mission of Mars Global Surveyor in elevation bins from 90°N to 90°S between 180°E and ~240°E.

containing TARs are grouped into the following ten formations: Channel System Materials (Achp, Hch, Hchp, Hcht); Olympus Mons Formation (Aoa_4, Aoa_1, Aoa_3, Aos); Ridged Plains Materials (Hr); Plateau Sequence (Npl_1, Npl_2, Nplh, Nplr, Hpl_3); Tharsis Formation (Ht_1, AHt_3, At_4, Ht_2); Highly Deformed Terrain Materials (v, HNu, Nb, Nf); Medusae Fossae Formation (Aml, Amm, Amu); Impact Crater Materials (cb, cs, s); Arcadia Formation (Aa_1, Aa_3, Aa_4); and Surficial Materials (Ad, Adl, Ae, Am, Api, Apl, As). The total number of images from each group ranges from 74 in the Channel System Materials to 1344 in the Plateau Sequence, (average = 461; SD = 495). The number of images with TARs from each group ranges from 20 in the Impact Crater Materials to 225 in the Plateau Sequence (average = 52; SD = 62). The cumulative area of the units within each formation containing TARs ranges from 156,600 km^2 to 5,515,100 km^2 (average = 1,709,000 km^2; SD = 1,767,300 km^2).

[33] The percent of images with TARs in each formation ranges from 3–39% (average = 17%; SD = 11%, Figure 6). The greatest frequency of images with TARs occurs in the Channel System Materials (39%) and the Olympus Mons Formation (33%), likely indicating the importance of numerous topographic traps within these terrains. The frequency of images with TARs for the remaining formations are <20%, with the lowest values occurring in the Arcadia Formation and Surficial Materials (4% and 3%, respectively). Image density (total number of images in each formation/cumulative area of units in each formation) is a parameter that provides a relative sense of the area captured by the images from each formation (see section 3 for further discussion). The image density for each geomorphic group ranges from 0.00007 for the Olympus Mons Formation to 0.0012 for the Impact Crater Materials (average = 0.00041; SD = 0.00038).

[34] The following 15 units from the study region did not contain any images with TARs: Vastitas Borealis Formation (Hvk, Hvm, Hvr); Alba Patera Formation (Aam, Hal); Dorsa Argentea Formation (Hdu); Elysium Formation (d); Aa_2 and Aa_5 in the Arcadia Formation; Npld and Nple in the Plateau Sequence; Aop in the Olympus Mons Formation; Hf and m in the Highly Deformed Terrain Materials; and Ach in the Channel System Material. The total number of images from these units and formations range from 1 in the Dorsa Argentea Formation and Elysium Formation to 181 in the Vastitas Borealis Formation (average = 51; SD = 62). The cumulative area of these units ranges from 7,400 km^2 to 820,200 km^2 (average = 236,100 km^2; SD = 292,900 km^2). The image density for units or formations without TARs is 0.0001 to 0.0003 (average = 0.00021; SD = 0.00008). Although the total number of images examined from these units and formations are far fewer relative to the formations with TARs, their surface areas are much smaller so their image densities are roughly comparable (Figure 6).

[35] The conditions that facilitate the formation of aeolian bedforms are sufficient sediment supply, adequate wind velocity and low surface roughness. The prevalence of TARs in geologic units at elevations above the relatively smooth northern lowlands correlate to materials displaying considerable topographic relief and many depressions that can serve as sediment traps. The presence of local and regional topography affects wind velocity and direction, which can enhance erosion and sediment transport [*Greeley et al.*, 2002]. In a modeling study of aeolian bedforms in troughs on Mars, *Bourke et al.* [2004b] show that wind velocities increase by ~30% on the downwind side of trough margins, indicating that inclined locations are more likely to exceed the threshold wind speed required for sediment transport. Most images with TARs are found in low-standing areas such as Newton Crater, Gorgonum Chaos and Atlantis Chaos as well as the floors of extensional grabens and troughs including the Sirenum Fossae and Memnonia Fossae systems in Terra Sirenum and the Olympus Mons Aureole. Since topographic traps appear to

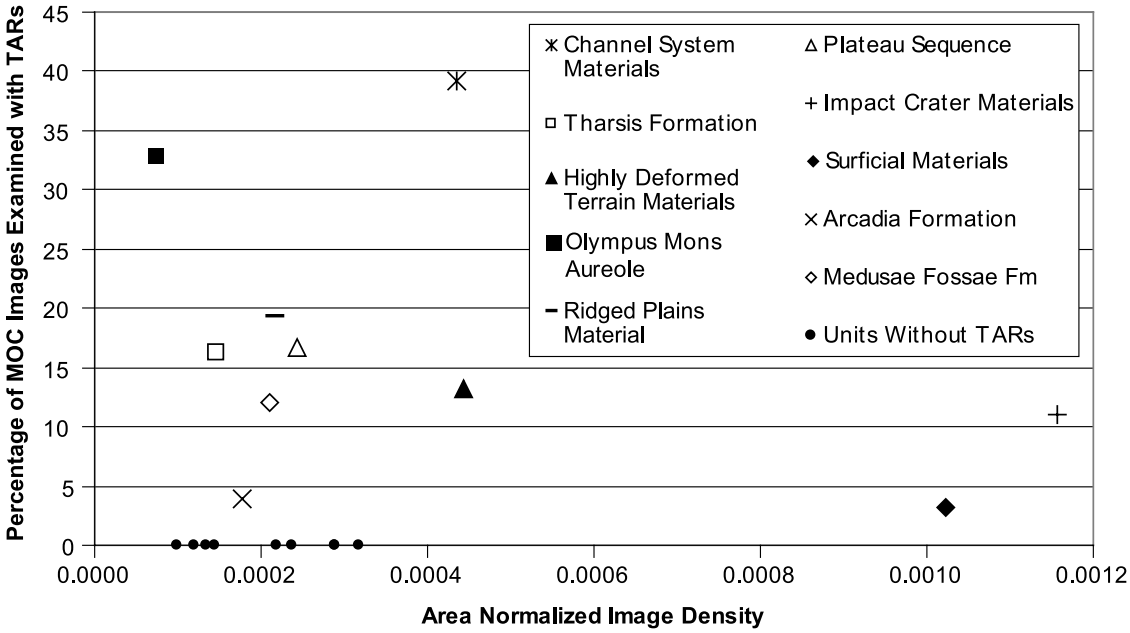

Figure 6. Percentage of examined MOC NA images with transverse aeolian ridges (TARs) in each geologic formation versus image density (total number of images per formation/cumulative area of units within each formation). The following units are associated with each formation: Channel System Materials (Achp, Hch, Hchp, Hcht); Olympus Mons Formation (Aoa_4, Aoa_1, Aoa_3, Aos); Ridged Plains Materials (Hr); Plateau Sequence (Npl_1, Npl_2, Nplh, Nplr, Hpl_3); Tharsis Formation (Ht_1, AHt_3, At_4, Ht_2); Highly Deformed Terrain Materials (v, HNu, Nb, Nf); Medusae Fossae Formation (Aml, Amm, Amu); Impact Crater Materials (cb, cs, s); Arcadia Formation (Aa_1, Aa_3, Aa_4); and Surficial Materials (Ad, Adl, Ae, Am, Api, Apl, As).

enhance the development of TARs along the floors of these low-lying depressions, geologic units such as the Channel System Materials (Achp, Hch, Hchp, Hcht) and the Olympus Mons Formation (Aoa_4, Aoa_1, Aoa_3, Aos) that are characterized by troughs, valleys, grabens, faults and scarps typically contain the highest frequency of TARs. Although the presence of TARs in channels and topographic depressions might suggest a local sediment source, MOC images do not provide conclusive evidence to support or disprove this hypothesis. *Bourke et al.* [2004b] suggest that the trough floors may be a sediment source for transverse ridges in linear depressions, and other researchers also propose a local source [*Fenton et al.*, 2003]. The TARs associated with the Olympus Mons Aureole may indicate a local volcanic sediment source, but the pervasive dust cover precludes testing this hypothesis using TES and THEMIS data. The relative paucity of TARs near Elysium suggests that volcanic material may not be a source for TARs in this area, or the volcanic activity associated with Elysium Mons is sufficiently older than Tharsis so that sand-sized particles are not available in this region.

4.5. Local Slope and Surface Roughness

[36] Since TARs tend to occur on flat-lying surfaces on the floors of steep-sided troughs and craters, we analyzed slopes at 1.85 km/pixel to represent the effects of small-scale, local topography that likely has the greatest influence on the development of these bedforms. Slope values were calculated at 1.85 km/pixel for all images from 60°N to 60°S between 180°E to ~240°E, resulting in slope values for 483 images with TARs and 2510 images without TARs. The images with and without TARs have average slopes of 1.92° (SD = 0.12°) and 1.36° (SD = 0.04°), respectively. The difference between average slope values for images with and without TARs is statistically significant (p-value <0.001). The slope values correspond to the latitude and longitude point at the center of each MOC image, which does not necessarily represent the exact location of the TARs in the image. The mean slope values for images without TARs represent a myriad of terrains from the smooth northern lowlands to the cratered highlands. The slightly higher average slope values of MOC images with TARs is possibly influenced by the high frequency of TARs at the bottom of steep-sided depressions in the Olympus Mons Aureole and the lack of TARs in the lowlands. In order to better understand the relationship between slopes, roughness and the distribution of TARs, we qualitatively assessed the distribution of TARs in relation to surface roughness and quantitatively analyzed the frequency of TARs in specific geologic units of known roughness (as described by *Kreslavsky and Head* [1999, 2000]).

[37] *Kreslavsky and Head* [2000] mapped the kilometer-scale surface roughness from MOLA data using long, intermediate and small-scale baseline lengths of 19.2 km, 2.4 km and 0.6 km, respectively. They found latitudinal trends of roughness in both hemispheres and distinctive roughness characteristics associated with several geologic units. In general, the southern hemisphere of Mars is rough at all scales, but the equatorial region has a ~3 times larger small-scale (0.6-km baseline length) roughness than high southern latitudes. In the study region, this latitudinal roughness trend is delineated by a smoothed terrain boundary

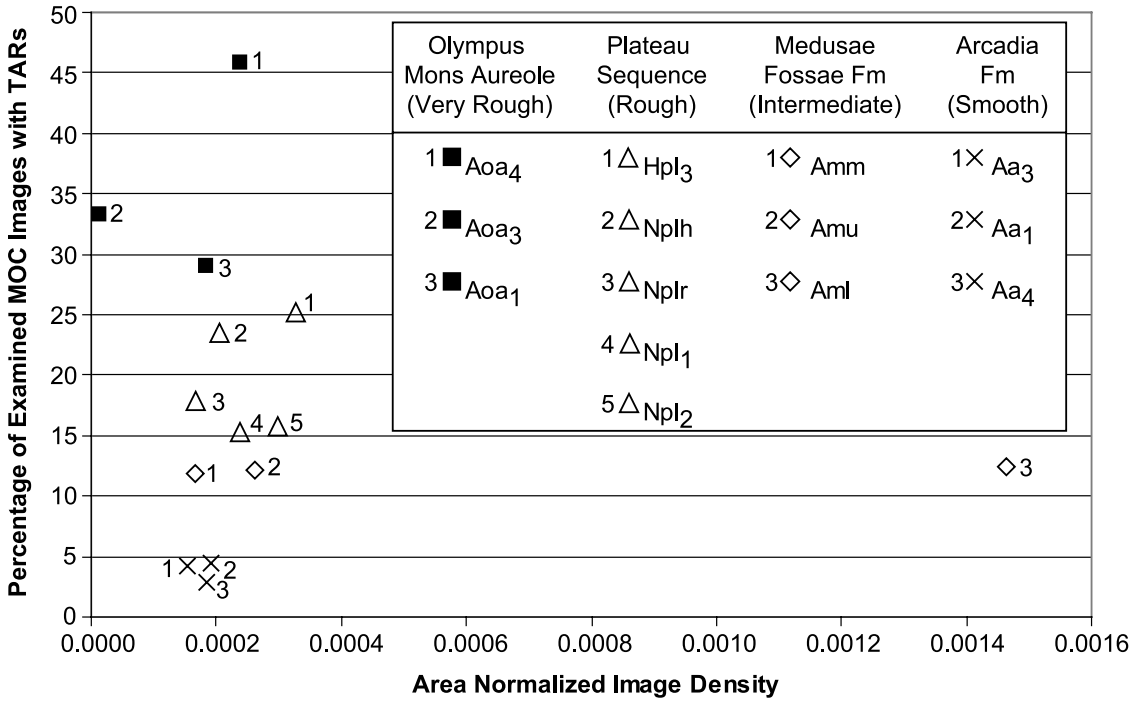

Figure 7. Percentage of examined MOC NA images with transverse aeolian ridges (TARs) versus image density (total number of images per formation/cumulative area of units within each formation) for select geologic formations across a range of surface roughness values.

around 50°S, which directly corresponds to a significant decrease in the occurrence of TARs poleward of this boundary. The difference in the characteristic vertical scale along this boundary is estimated to be on the order of several meters on the basis of model data [*Kreslavsky and Head*, 2000]. Similar to the southern hemisphere, the northern hemisphere exhibits a relative decrease (~2–3 times) in small-scale roughness around 47°, although this boundary is not well defined in the study region. The study region in the northern hemisphere has smooth surfaces associated with Arcadia and Amazonis Planitia. From the equator to roughly 40°N, this smooth region with few TARs is bound by regions of high surface roughness that correlate to the Olympus Mons Aureole (between 210° and 240°E) and the knobby and ridged terrain in eastern Elysium. These rough areas in the northern hemisphere directly correlate to high occurrences of TARs.

[38] The latitudinal trend in roughness is due to the presence of a high-latitude debris mantle that is between 1 and 10 meters thick [*Kreslavsky and Head*, 2000; *Mustard et al.*, 2001]. *Mustard et al.* [2001] suggest the deposit is a layer of cemented dust that was emplaced in the last 0.15 Myr and is undergoing desiccation, disaggregation and removal. The emplacement of this mantling layer is thought to be related to a series of climate-driven cycles resulting from changes in obliquity [*Kreslavsky and Head*, 2000; *Mustard et al.*, 2001], the most recent of which occurred in the last ~2.1 to 0.4 Myr [*Head et al.*, 2003]. Unlike the thin dust cover draped over TARs in regions of low TI (section 4.3), a mantling deposit up to 10 m in thickness could completely bury TARs that are thought to be on the order of ~2 to ~6 m in height [*Williams and Zimbelman*, 2003; *Wilson et al.*, 2003; *Bourke et al.*, 2004a].

[39] *Kreslavsky and Head* [2000] identified characteristic roughness values of several geologic units including Aoa_4, Aoa_3 and Aoa_1 of the Olympus Mons Formation, Npl_1 from the Plateau Sequence in the southern highlands, the Medusae Fossae Formation and Aa_3 from the Arcadia Formation in the northern hemisphere. The upper member of the Olympus Mons Aureole, Aoa_4, is the roughest terrain on Mars (at all scales with a maximum at ~2.5-km baseline length). This unit forms broad, circular, flat lobes consisting of numerous faults, scarps, and deep troughs and grabens [*Scott and Tanaka*, 1986]. The Aoa_3 member of the Olympus Mons Aureole has a similar characteristic spatial scale of topography relative to the Aoa_4 member, but is slightly less rough. The Aoa_1 member is essentially smoother than both Aoa_4 and Aoa_3, with a shorter characteristic spatial scale of topography. The Npl_1 unit from the highlands is characterized by craters with smooth floors and steep walls, resulting in rough, spotty terrain at all scales. The surface of the Medusae Fossae Formation is relatively rougher than the northern lowlands and smoother than the equatorial highlands. Lastly, the Aa_3 member of the Arcadia Formation is very smooth. On the basis of the relative surface roughness of the Olympus Mons Aureole (very rough), the Plateau Sequence (rough), Medusae Fossae Formation (intermediate roughness) and Arcadia Formation (smooth), we compared the frequency of TARs from each unit in the aforementioned formations (Figure 7). There is a positive linear correlation ($R^2 = 0.87$) between the frequency of images with TARs and relative surface roughness associated with specific geologic units. As surface roughness decreases from Aoa_4 to Aoa_3 to Aoa_1, the percentage of images with TARs systematically decreases

(46%, 33% and 29%, respectively). The frequency of images with TARs from presumably rough units in the Plateau Sequence (Hpl_3, Nplh, Nplr, Npl_1 and Npl_2) ranges from 15–25%. The frequency of TARs from units in the Medusae Fossae Formation (Amm, Amu and Aml) identified as ''intermediate'' roughness range from 12–13%. The smooth units in the Arcadia Formation (Aa_3, Aa_1, and Aa_4) have the lowest frequency of TARs (3–4%). Therefore the frequency of TARs in geologic units and formations appears to be directly related to (small-scale) surface roughness, and the availability of sediment traps associated with this roughness.

5. Conclusions and Future Work

[40] The study area (90°N to 90°S between 180°E and ~240°E) characterizes approximately 15% of the Martian surface. Although the coverage of MOC images examined from the primary mission clearly does not capture the entire surface of this region, the data are sufficient to make first-order observations about the location of transverse aeolian ridges (TARs) and their relationship to latitude, elevation, thermal inertia, geologic units, local slopes and surface roughness. Interpretations from this regional study are based on the assumptions that images are relatively evenly targeted throughout the area of interest and the surface area captured by each image is comparable.

[41] Transverse ridges occur in 10% of the images examined, indicating the prevalence of these aeolian bedforms on the surface of Mars. These features predominantly occur between 40°N and 50°S, and are not prevalent in the mid- to upper latitudes or the polar regions of either hemisphere. The concentration of TARs in the equatorial and midlatitudes may signal enhanced sediment abundance or increased wind speeds at lower latitudes rather than a lack of such components nearer to the poles. Of the parameters investigated in this study, the latitudinal trend appears to be predominantly related to surface roughness. These distinct aeolian bedforms commonly occur at elevations above the northern lowlands with the highest frequency in rough terrain characterized by abundant low-lying depressions such as crater, trough and graben floors.

[42] The latitudes, elevations, geologic units, and areas of thermal inertia that lack the presence of TARs in MOC NA images certainly does not preclude the occurrence of active aeolian processes in these areas. TAR formation at some locations may be hindered by an inadequate supply of particles capable of being moved by the wind, or winds of insufficient intensity or duration to support their development. The observed paucity of TARs in some areas may be a result of poor MOC image resolution (>10 m/pixel), quality or coverage. Even the excellent resolution of the MOC NA images does not appear to be sufficient to provide definitive evidence that TARs are formed by either saltation or reptation processes. These results are applicable only to images from the primary mission, so further examination of recently released, high resolution MOC NA images in the study area might minimize the effects of poor image quality, but should not alter the basic results reported here. Similar studies of other regions on Mars would elucidate any regional variations in TARs and their relationship to surface roughness on a large scale. Additional local and regional investigations of TARs are necessary to further constrain age, physical characteristics (i.e., grain size, density), source material and formational processes. Enhanced understanding of these properties may help decipher the global wind regime and climate in which TARs formed or were subsequently modified.

[43] **Acknowledgments.** Thank you to Ross Irwin for help with GIS and data processing and to Peter Thomas and A. W. Ward for constructive and insightful reviews that greatly improved this manuscript. The authors acknowledge the use of Mars Orbiter Camera images processed by Malin Space Science Systems that are available at http://www.msss.com/moc_gallery/. This research was supported by NASA MDAP grant NAG5-11075.

References

Anderson, R. S. (1987), A theoretical model for aeolian impact ripples, *Sedimentology*, *34*, 943–956.

Anderson, R. S., and P. K. Haff (1988), Simulation of eolian saltation, *Science*, *241*, 820–823.

Bagnold, R. A. (1941), *The Physics of Blown Sand and Desert Dunes*, 265 pp., Methuen, New York.

Bell, J. F., P. C. Thomas, M. J. Wolff, S. W. Lee, and P. B. James (1997), Mineralogy of the Martian north polar sand sea from 1995 Hubble Space Telescope near-IR observations, *Proc. Lunar Planet. Sci. Conf. 28th*, 87–88.

Bourke, M. C., S. A. Wilson, and J. R. Zimbelman (2003), The variability of TARs in troughs on Mars, *Lunar Planet. Sci.* [CD-ROM], *XXXIV*, abstract 2090.

Bourke, M. C., M. Blame, R. A. Beyer, K. K. Williams, and J. Zimbelman (2004a), How high is that dune? A comparison of methods used to constrain the morphometry of aeolian bedforms on Mars, *Lunar Planet. Sci.*, *XXXV*, abstract 1713.

Bourke, M. C., J. E. Bullard, and O. S. Barnouin-Jha (2004b), Aeolian sediment transport pathways and aerodynamics at troughs on Mars, *J. Geophys. Res.*, *109*, E07005, doi:10.1029/2003JE002155.

Breed, C. S. (1977), Terrestrial analogs of the Hellespontus dunes, Mars, *Icarus*, *30*, 326–340.

Breed, C. S., M. J. Grolier, and J. F. McCauley (1979), Morphology and distribution of common ''sand'' dunes on Mars: Comparison with the Earth, *J. Geophys. Res.*, *84*, 8183–8204.

Carr, M. H., and M. C. Malin (2000), Meter-scale characteristics of Martian channels and valleys, *Icarus*, *146*(2), 366–386.

Christensen, P. R. (1986), Regional dust deposits on Mars: Physical properties, age and history, *J. Geophys. Res.*, *91*(B3), 3353–3545.

Cooke, R. U., and A. Warren (1973), *Geomorphology in Deserts*, 394 pp., Batsford, London.

Cooke, R., A. Warren, and A. Goudie (1993), *Desert Geomorphology*, 526 pp., UCL Press, London.

Cutts, J. A., and R. S. U. Smith (1973), Eolian deposits and dunes on Mars, *J. Geophys. Res.*, *78*, 4139–4154.

Cutts, J. A., K. R. Blasius, G. A. Briggs, M. H. Carr, R. Greeley, and H. Masursky (1976), North polar region of Mars: Imaging results from Viking 2, *Science*, *194*, 1329–1337.

Edgett, K. S. (1997), Aeolian dunes as evidence for explosive volcanism in the Tharsis region of Mars, *Icarus*, *130*, 96–114.

Edgett, K. S. (2002), Low-albedo surfaces and eolian sediment: Mars Orbiter Camera views of western Arabia Terra craters and wind streaks, *J. Geophys. Res.*, *107*(E6), 5038, doi:10.1029/2001JE001587.

Edgett, K. S., and M. C. Malin (2000a), Eolian bedforms and erosional landforms at high altitudes on the Martian Tharsis volcanoes, *Lunar Planet. Sci.* [CD-ROM], *XXXI*, abstract 1072.

Edgett, K. S., and M. C. Malin (2000b), New views of Mars eolian activity, materials, and surface properties: Three vignettes from the Mars Global Surveyor Mars Orbiter Camera, *J. Geophys. Res.*, *105*, 1623–1650.

Edgett, K. S., and T. J. Parker (1998), ''Bright'' aeolian dunes on Mars: Viking Orbiter observations, *Lunar Planet. Sci.* [CD-ROM], *XXIX*, abstract 1338.

Ellwood, J. M., P. D. Evans, and I. G. Wilson (1975), Small scale aeolian bedforms, *J. Sediment. Petrol.*, *45*, 554–561.

Fenton, L. K., J. L. Bandfield, and A. W. Ward (2003), Aeolian processes in Proctor Crater on Mars: Sedimentary history as analyzed from multiple data sets, *J. Geophys. Res.*, *108*(E12), 5129, doi:10.1029/2002JE002015.

Fryberger, S. G., P. A. Hesp, and K. Hastings (1992), Aeolian granule ripple deposits, Namibia, *Sedimentology*, *39*, 319–331.

Greeley, R., and J. E. Guest (1978), Geologic map of the eastern equatorial region of Mars, *U.S. Geol. Surv. Misc. Invest. Ser.*, *Map I-1802–B*, scale 1:15,000,000.

Greeley, R., and J. D. Iversen (1985), *Wind as a Geological Process on Earth, Mars, Venus and Titan*, 333 pp., Cambridge Univ. Press, New York.

Greeley, R., M. D. Kraft, R. O. Kuzmin, and N. T. Bridges (2000), Mars Pathfinder landing site: Evidence for a change in wind regime from lander and orbiter data, *J. Geophys. Res.*, *105*, 1829–1840.

Greeley, R., N. T. Bridges, R. O. Kuzmin, and J. E. Laity (2002), Terrestrial analogs to wind-related features at the Viking and Pathfinder landing sites on Mars, *J. Geophys. Res.*, *107*(E1), 5005, doi:10.1029/2000JE001481.

Greeley, R., et al. (2004), Coordinated observations of aeolian features from the Mars Exploration Rovers (MER) and the Mars Express High Resolution Stereo Camera and other orbiters, *Lunar Planet. Sci.* [CD-ROM], *XXXV*, abstract 2162.

Head, J. W., J. F. Mustard, M. A. Kreslavsky, R. E. Milliken, and D. R. Marchant (2003), Recent ice ages on Mars, *Nature*, *426*, 797–802.

Kreslavsky, M. A., and J. W. Head (1999), Kilometer-scale slopes on Mars and their correlation with geologic units: Initial results from Mars Orbiter Laser Altimeter (MOLA) data, *J. Geophys. Res.*, *104*(E9), 21,911–21,924.

Kreslavsky, M. A., and J. W. Head (2000), Kilometer-scale roughness of Mars: Results from MOLA data analysis, *J. Geophys. Res.*, *105*(E11), 26,695–26,733.

Lancaster, N. (1994), Dune morphology and dynamics, in *Geomorphology of Desert Environments*, pp. 474–505, Chapman and Hall, New York.

Lancaster, N. (1995), *Geomorphology of Desert Dunes*, 290 pp., Routledge, New York.

Lee, S. W. (1986), IRTM observations of Syrtis Major: An active aeolian environment (abstract), in *Reports of Planetary Geology and Geophysics Program 1985*, *NASA Tech. Memo. 8*, *383*, 532–534.

Malin, M. C., and K. S. Edgett (2001), The Mars Global Surveyor Mars Orbiter Camera: Interplanetary cruise through primary mission, *J. Geophys. Res.*, *106*, 23,429–23,570.

Malin, M. C., G. E. Danielson, A. P. Ingersoll, H. Masursky, J. Veverka, M. A. Ravine, and T. A. Soulanille (1992), Mars Observer Camera, *J. Geophys. Res.*, *97*, 7699–7718.

Malin, M. C., et al. (1998), Early views of the Martian surface from the Mars Orbiter Camera of Mars Global Surveyor, *Science*, *279*, 1681–1685.

McCauley, J. F., M. H. Carr, J. A. Cutts, W. K. Hartmann, H. Masursky, D. J. Milton, R. P. Sharp, and D. E. Wilhelms (1972), Preliminary Mariner 9 report on the geology of Mars, *Icarus*, *17*, 289–327.

Mellon, M. T., B. M. Jakosky, H. H. Kieffer, and P. R. Christensen (2000), High-resolution thermal inertia mapping from the Mars Global Surveyor Thermal Emission Spectrometer, *Icarus*, *148*, 437–455.

Mellon, M. T., K. A. Dretke, M. D. Smith, and S. M. Pelkey (2002), A global map of thermal inertia from Mars Global Surveyor mapping-mission data, *Lunar Planet. Sci.* [CD-ROM], *XXXIII*, abstract 1416.

Mustard, J. F., C. D. Cooper, and M. K. Rifkin (2001), Evidence for recent climate change on Mars from the identification of youthful near-surface ground ice, *Nature*, *412*, 411–414.

Parker, T. J., R. S. Saunders, and D. M. Schneeberger (1989), Transitional morphology in West Deuteronilus Mensae, Mars: Implications for modification of the lowland/upland boundary, *Icarus*, *82*, 111–145.

Parker, T. J., D. S. Gorsline, R. S. Saunders, D. C. Pieri, and D. M. Schneeberger (1993), Coastal geomorphology of the Martian northern plains, *J. Geophys. Res.*, *98*, 11,061–11,078.

Peterfreund, A. R. (1985), Contemporary aeolian processes on Mars: Local dust storms, Ph.D. dissertation, 246 pp., Ariz. State Univ., Tempe.

Putzig, N. E., M. T. Mellon, and R. E. Arvidson (2003), Thermophysical properties of the Martian south polar region, paper presented at Sixth International Conference on Mars, Lunar and Planet. Inst., Houston, Tex.

Pye, K. (1987), *Aeolian Dust and Dust Deposits*, 334 pp., Academic, San Diego, Calif.

Pye, K., and H. Tsoar (1990), *Aeolian Sand and Sand Dunes*, 393 pp., Chapman and Hall, New York.

Sagan, C., et al. (1972), Variable features on Mars, 2. Mariner 9 global results, *J. Geophys. Res.*, *78*, 4163–4196.

Scott, D. H., and K. L. Tanaka (1986), Geologic map of the western equatorial region of Mars, *U.S. Geol. Surv. Misc. Invest. Ser.*, *Map I-1802–A*, scale 1:15,000,000.

Seppälä, M., and K. Linde (1978), Wind tunnel studies of ripple formation, *Geogr. Ann.*, *60*, 29–42.

Sharp, R. P. (1963), Wind ripples, *J. Geol.*, *71*, 617–636.

Smith, D. E., et al. (1999), The global topography of Mars and implications for surface evolution, *Science*, *284*, 495–1503.

Tanaka, K. L., and D. H. Scott (1987), Geologic map of the polar regions of Mars, *U.S. Geol. Surv. Misc. Invest. Ser.*, *Map I-1802–C*, scale 1:15,000,000.

Thomas, P. (1984), Martian intercrater splotches: Occurrence, morphology, and colors, *Icarus*, *57*, 205–227.

Thomas, P., and C. Weitz (1989), Sand dune materials and polar layered deposits on Mars, *Icarus*, *81*, 185–215.

Thomas, P. C., et al. (1999), Bright dunes on Mars, *Nature*, *397*, 592–594.

Tsoar, H. (1990), Grain size characteristics of wind ripples on a desert seif dune, *Geogr. Res. Forum*, *10*, 37–50.

Walker, D. J. (1981), An experimental study of wind ripples, M.Sc., Mass. Inst. of Technol., Cambridge.

Ward, A. W., K. B. Doyle, P. J. Helm, M. K. Weisman, and N. E. Witbeck (1985), Global map of aeolian features of Mars, *J. Geophys. Res.*, *90*, 2038–2056.

Werner, B. T. (1988), A steady-state model of wind-blown sand transport, *J. Geol.*, *98*, 1–17.

White, B. (1979), Soil transport by winds on Mars, *J. Geophys. Res.*, *84*(B9), 4643–4651.

Williams, K. K., and J. R. Zimbelman (2003), First measurements of ripple heights on Mars, *Geol. Soc. Am. Abstr. Programs*, *35*(6), abstract 67–1.

Williams, S. H., and J. R. Zimbelman (2002), Large ripple-like bedforms: Examples from Earth, *Geol. Soc. Am. Abstr. Programs*, *34*, abstract 77–7.

Williams, S. H., J. R. Zimbelman, and A. W. Ward (2002), Large ripples on Earth and Mars, *Lunar Planet. Sci.* [CD-ROM], *XXXIII*, abstract 1508.

Wilson, I. (1972a), Sand waves, *New Sci.*, *53*, 634–637.

Wilson, I. G. (1972b), Aeolian bedforms: Their development and origins, *Sedimentology*, *19*, 173–210.

Wilson, S. A., and J. R. Zimbelman (2002), Large ripple-like bedforms: Examples from the Mars Orbiter Camera, *Geol. Soc. Am. Abstr. Programs*, *34*, abstract 77–8.

Wilson, S. A., J. R. Zimbelman, and S. H. Williams (2003), Large aeolian ripples: Extrapolations from Earth to Mars, *Lunar Planet. Sci.* [CD-ROM], *XXXIV*, abstract 1862.

Zimbelman, J. R. (1987), Spatial resolution and the geologic interpretation of Martian morphology: Implications for subsurface volatiles, *Icarus*, *71*, 257–267.

Zimbelman, J. R. (2000), Non-active dunes in the Acheron Fossae region of Mars between the Viking and Mars Global Surveyor eras, *Geophys. Res. Lett.*, *27*(7), 1069–1072.

Zimbelman, J. R. (2003), Decameter-scale ripple-like features in Nirgal Vallis as revealed in THEMIS and MOC imaging data, paper presented at Sixth International Conference on Mars, Lunar and Planet. Inst., Houston, Tex.

Zimbelman, J. R., and S. A. Wilson (2002), Ripples and dunes in the Syrtis Major region of Mars, as revealed in MOC images, *Lunar Planet. Sci.* [CD-ROM], *XXXIII*, abstract 1514.

S. A. Wilson, Department of Environmental Sciences, University of Virginia, Charlottesville, VA 22904-4123, USA. (sharonwilson@virginia.edu)

J. R. Zimbelman, Center for Earth and Planetary Studies, National Air and Space Museum, MRC 315, Smithsonian Institution, Washington, DC 20013-7012, USA. (zimbelmanj@nasm.si.edu)